Development of a New Methodology for Evaluation of Beam Accuracy and Optical Quality of Solar Central Receiver Systems

Mohamed Adel*‡, Adrian Peña-Lapuente**, Mohamed Rady***, Alaa Hamdy****

*Mechanical Engineering Department, Helwan University, 11792 Helwan, Cairo, Egypt

**Solar Thermal Department, National Renewable Energy Centre of Spain (CENER), 31621 Sarriguren, Navarra, Spain

***Mechanical Engineering Department, Faculty of Engineering, Rabigh, King Abdulaziz University, KSA

****Electronics, Communications and Computer Engineering Department, Helwan University, 11792 Helwan, Cairo, Egypt

(m.adel_helwan@yahoo.com, apena@cener.com, maradhi@kau.edu.sa, alaa.hamdy@gmail.com)

‡ Corresponding Author; Mohamed Adel, 1 Sherif Street, 11792 Helwan, Cairo, Egypt, Tel: +20 109 077 6722, m.adel_helwan@yahoo.com

Received: 13.03.2021 Accepted: 21.04.2021

Abstract- In central tower concentrated solar power plants, the concentrated flux distribution at the receiver is controlled by the aiming strategy of thousands of heliostats in the field to accomplish the specific requirements of solar-thermal conversion processes. The main goal of this work is to evaluate the reflected solar flux from a heliostat or from a group of heliostats on a calibration target. The solar flux map at the target receiver is constructed using the information embedded in a captured high dynamic range image of the evaluated scene. In the present article, a methodology has been proposed to evaluate the optical performance of solar central receiver systems in terms of beam accuracy and optical quality of reflected light on calibration target. The developed system is a simple, automatic and effective tool used to accurately analyse the reflected solar flux without limitations of previous methods, such as using specific type of calibration target. The capability of the present methodology for accurate analysis is demonstrated through experimental indoor and outdoor tests.

Keywords- Beam accuracy; Optical Quality; Heliostat; Image-Based Solar Flux Analysis.

Nomenclature

ADC	Average of deviations in captured image
ADCM	Ratio between average of deviations and maximum pixel value in captured image
ADR	Average of deviations in reference image
ADRM	Ratio between average of deviations and maximum pixel value in reference image
b	Shift value
BW	Black and white
CCD	Charge-Coupled Device
DC	Deviation of pixel value from maximum pixel value in captured image
DR	Deviation of pixel value from maximum pixel value in reference image
Error %	Distribution error percentage
HDR	High Dynamic Range
h_{max}	Most representative intensity value
m	Number of pixels in captured image
n	Number of pixels in reference image
SCR	Solar Central Receiver
TH	Threshold value
y	Pixel value
yc	Pixel value in captured image
yc_{max}	Maximum pixel value in captured image
y_{max}	Maximum pixel value in grayscale image
yr	Pixel value in reference image
yr_{max}	Maximum pixel value in reference image

1. Introduction

The operation of solar central receiver (SCR) plants requires high precision in the point of the reflection of solar rays by the heliostats field towards the receiver target. The

usual practice in heliostat field characterization and calibration is to command the specified heliostat to direct its radiation on a special target beside the central receiver [1]. The sunspot of each single heliostat is then analysed and evaluated. Experimental evaluation and measurement methods of incident solar flux are classified into direct and indirect methods [2]. Indirect measurement principles are being used since the end of the 1970s [3]. In [2], [4] and [5], characterization methods using diffuse moving bar target and digital camera to characterize the flux distribution reflected on the central receiver by all heliostats at the same time have been presented. A method using digital camera directly on the receiver surface has been presented in [6]. A stationary stripe-shaped target and digital camera have been used in the method presented in [7]. For evaluation of global solar radiation data, different methods have been presented in [8-10]. In [11] and [12], experimental methods for evaluation of solar flux and its effect on the performance of the system have been presented. As illustrated in the literature presented in [2] and [3], indirect methods usually use digital cameras to characterize flux distributions. Cameras are used to image the flux distribution of the reflected light which is then analysed. The information extracted from the reflected image is very useful for calibration and control of plant operation.

High quality operation of heliostats requires precise knowledge of the reflected beam accuracy to orient the system adequately for reflecting the sun onto a specific point on the central receiver. So, beam accuracy is a measure of the tracking system accuracy. Tracking accuracy improvements may significantly increase the power plant performance [13]. This accuracy is usually known after construction due to slight variations in the fabricated parts and the final assembly. Also, the optical quality is crucial for accurate determination of the total energy sum and its distribution and concentration on the receiving plane. The optical quality of heliostats has a significant impact on the overall efficiency of SCR plants because the major cost component in the plant is the heliostat field [14]. Therefore, accurate estimation systems are needed to detect optical deficiencies in the system to improve the heliostats optical quality. To ensure high optical quality, the flux distribution on the receiver of the system has to be congruent with the ideal designed distribution.

For accurate analysis, image-based solar flux analysis systems require high dynamic range (HDR) images that contain all details of low and high illumination areas of the captured solar flux. In the present work, an image-based SCR optical analysis methodology, which is considered as a powerful tool for accurate analysis of incident solar flux on receivers of SCR systems, is presented. In practice, analysis results are used for heliostat calibration. It also could serve as feed-back information for adjustment purposes of heliostat tracking and control systems. In the present methodology, for all captured images, a calibrated double-CCD camera (JAI AD-081GE CCD) is used to capture two images of the same scene with different levels of exposure. When JAI control tool is executed, AD-081GE is recognized as two imagers that can be handled as independent cameras [15]. The JAI control tool is a software that is used for building vision systems for controlling JAI cameras. It can be used for testing and evaluation of JAI cameras [16]. Merging both images, using the technique presented in [17], results in obtaining an accurate HDR image that contains all details of the captured scene. Accurate HDR images lead to accurate solar flux analysis.

The major contribution of the present work can be summarised as follows:

- Development of a new technique for evaluation of incident solar flux on receivers of SCR systems in terms of optical quality and beam accuracy.
- Demonstration of the capability of the developed technique for accurate optical analysis of reflected solar flux in SCR systems.
- In addition to calibration and characterization, analysis results of the developed technique are very useful for accurate tracking and control of solar central receiver systems.

The present article is organised following the procedure adopted in developing the proposed methodology as follows. The beam accuracy evaluation method is described in Section 2. The beam accuracy is evaluated in a sequence of steps, where the target is extracted from captured HDR image, then the target centre is compared to the calculated centroid of the incident flux on the target to detect the amount of deviation. Section 3 discusses the proposed methodology for evaluation of the optical quality of SCR systems. The methodology evaluates the optical quality by calculating the error in solar flux distribution in the captured image as compared to the reference designed distribution. Investigation of the capability of the proposed methodology for optical analysis of SCR systems are reported in Section 4. Finally, Section 5 shows the procedures and results of outdoor test application.

2. Beam Accuracy

The tracking accuracy is frequently determined by the measured position of the reflected beam centre on a target [18]. The beam accuracy, also referred to as centering, is measured by the deviation of the centroid of the flux map from the well-known geometrical centre of the target. Beam accuracy calculation is based on target centre calculation, which is considered as the aiming point, and the solar spot centroid calculation. In the present work, the presented method for calculations of centroids of target and solar spot is similar to that is presented in [18]. The following sections present in detail the methodology of evaluation of beam accuracy of SCR systems.

2.1. Target Centre Calculation

In the present study, an algorithm has been developed to detect the target and calculate its centre using the captured image. The algorithm is executed in five main steps, starting with image capture step. Image histogram step is then performed, followed by applying thresholds step and then perspective correction process. Finally, target centre detection step is executed.

Applying thresholds step presented in the proposed methodology solves the problem of using specific type of targets in calibration processes, as will be illustrated in the following sections. The alignment between the centre of the camera lens and the calibration target centre in actual solar plants is a very difficult process. Therefore, perspective correction step presented in the present work is an important step that reduces errors in target centre and light spot centre calculations. Detailed description of the application of each step is explained in the following sections.

2.1.1.Image Capture

The position of the camera should be adjusted manually to show the target in the captured image. The captured images, using the double-CCD camera, are grayscale images. The target image is captured without reflected light on it, because the target detection step is done by determining the gray-level of the pixels that belongs to the target. An image for a flat plate was captured as a first approximation to the real target case as shown in Fig. 1.

2.1.2.Image Histogram

Image histogram is a representation of the distribution of intensity levels in the image [19]. For grayscale 8-bit image, the intensity level range varies between 0 and 255. The histogram of the captured image is calculated and the most representative intensity in the image is obtained. Fig. 2 shows the histogram of the image of Fig. 1.

Fig. 1. Image of flat plate captured with the double-CCD camera.

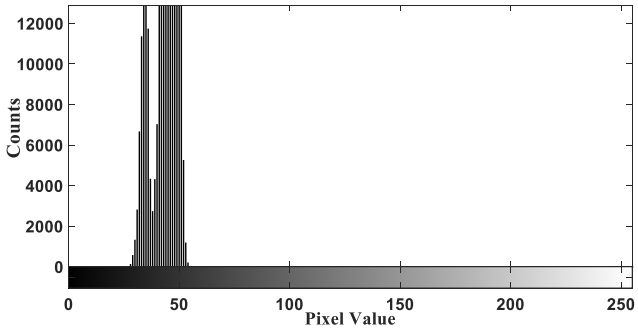

Fig. 2. Histogram of image of Figure 1.

2.1.3.Applying Thresholds

The technique of dividing a digital image into classes of pixels is called thresholding [20]. In the present work, the algorithm is based on applying thresholds in order to distinguish aiming pixels from other pixels. In this part of the sequence, aiming pixels refer to pixels of the target. All target pixels do not contain the same intensity value. This difference is due to distortions in the surface of the target. That is why, only some of them are used for threshold values selection. This also means that applying one threshold will ignore parts of the target. Therefore, two thresholds are used to segment the pixels of the target. Pixels that contain most representative intensity represent the main part of the target. If TH_1 is the first threshold value and TH_2 is the second threshold value, the two threshold values can be calculated using Eq. (1) and Eq. (2).

$$TH_1 = h_{max} + b \quad (1)$$

$$TH_2 = h_{max} - b \quad (2)$$

Where h_{max} is the most representative intensity value in the image histogram, and b is a shift value. The shift value has been obtained by a trial-and-error procedure using different experiments in different illumination levels. In the present work, the obtained shift value is 25, but is not a general recommendation, as it depends on the camera settings, as illustrated in [18]. Fig. 3a shows the target image after applying two thresholds. Applying thresholds converts the grayscale image to binary image, black and white (BW) image, by replacing pixels between TH_1 and TH_2 with the value 1 (white) and replacing all other pixels with the value 0 (black).

After obtaining a BW image, the connected components are defined. A connected component is a set of connected pixels that share a specific property. This is accomplished by finding a pixel with value 1 in the BW image, then looking at all its neighbours, labeling each pixel that has the same value as being in the same component, and so on. According to the number of connected pixels, the area of each component could be calculated. In our case, the component with the largest area is of interest as it represents the target surface. Fig. 3b shows the BW target image after ignoring small components. Fig. 3c shows the image after applying a Gaussian filter. The filter is applied to treat defects that may arise after thresholding.

2.1.4.Perspective Correction

For accurate calculation of the target centre, perspective correction for the plane of the target has to be done. Perspective is the projection of actual vision [21]. Parallel projection is needed because it facilitates the application of the regularities of centre calculation. MATLAB is used for performing this task. But the projective transformation is applied on coordinates of four corners. Depending on illumination variation, edges between pixels with value 1 and pixels with value 0 are detected. The four corners of interest are obtained by selecting the minimum and maximum values in the detected points array. All detected edges are illustrated

in Fig. 3d, while the four desired corners are illustrated in Fig. 3e. The position of the corners in the binary image is the same in the grayscale image. Therefore, the four corners are used for adjusting the projection of the grayscale image. Fig. 3f shows the grayscale image of the target after perspective correction.

2.1.5. Target Centre Detection

After getting a parallel projection, the target centre can be easily calculated. The central row of the target image is calculated, that is, the horizontal line crossing the centre of the target. The central column of the target image is calculated, that is, the vertical line crossing the centre of the target. The cross point between the central row and the central column is the target centre. The red mark in Fig. 3f refers to the position of the target centre.

Because, as discussed before, beam accuracy is measured by the deviation of the centroid of the solar flux map from the geometrical centre of the target, the following section discusses how to calculate the centroid of solar spot reflected on a target.

2.2. Solar Spot Centroid Calculation

The solar spot centroid is calculated in a similar way of calculating the target centre. Firstly, an image for a fixed flat plate was captured, perspective correction was done, and centre was calculated. Then, a lamp directed to form a spot on the flat plate was used to simulate the solar flux coming from a heliostat field, as a first approximation to the real case. Two grayscale images were captured at different exposure times for the light spot. The two images were merged into a HDR image using the proposed methodology presented in [17]. The position of the four corners used for perspective correction of the target image is the same for the spot image. Fig. 4a shows the merged image after perspective correction.

A threshold value is chosen and applied. The centroid of the segmented spot is calculated. It is calculated from the binary image and then applied to the original grayscale image. For spot segmentation, the threshold value is calculated using Eq. (3).

$$TH = 0.6 * y_{max} \tag{3}$$

Where TH is the threshold value and y_{max} is the maximum intensity value in the grayscale image. The location (row and column) of each pixel with value 1 in the binary image is calculated. The average of rows is the horizontal line crossing the centroid of the spot and the average of columns is the vertical line crossing the centroid of the spot. The cross point is the centroid point of the solar spot. Fig. 4b shows the segmented image of the light spot and Fig. 4c shows the location of the centroid of the spot on the original grayscale image.

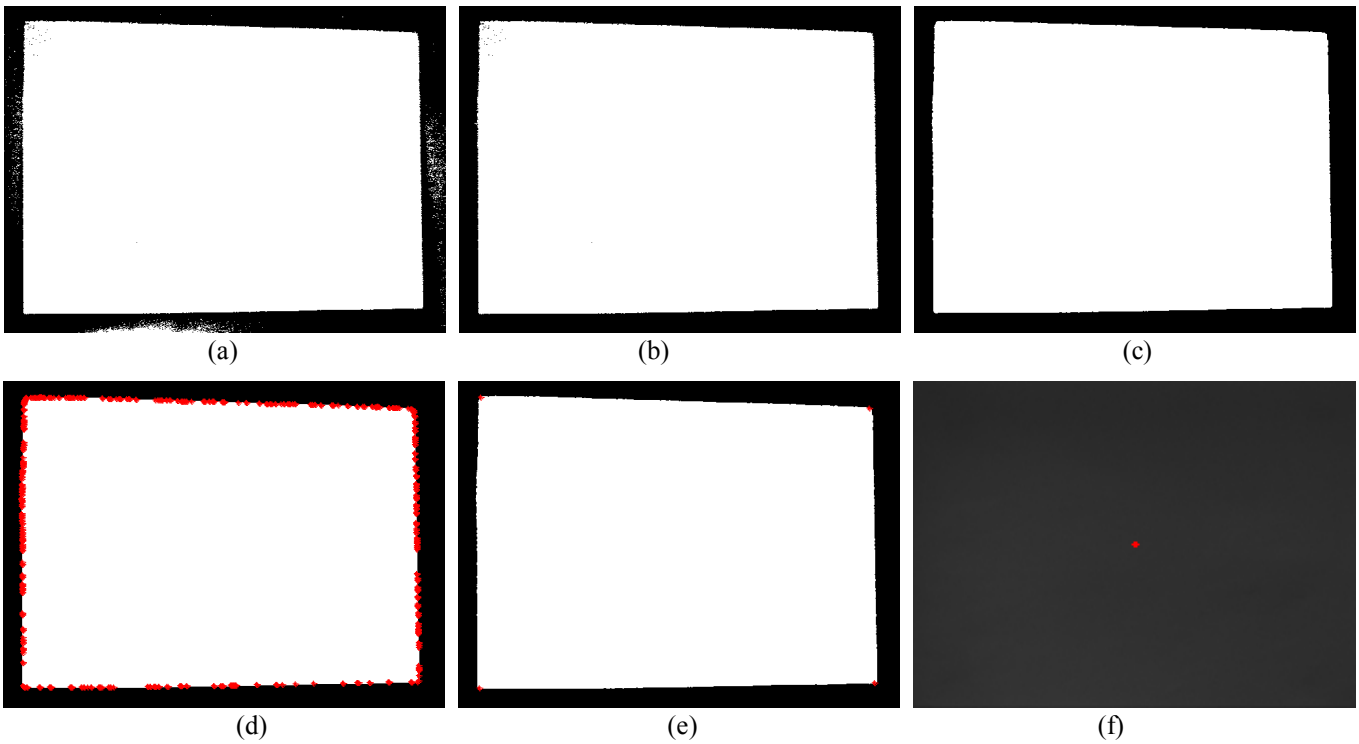

Fig. 3. (a) Target image after applying thresholds. (b) BW image after ignoring small components. (c) BW image after applying Gaussian filter. (d) BW image with all detected edges. (e) BW image with the four desired corners. (f) Target image after perspective correction (the marked point is the target centre).

If the target centre is considered as the aiming point, in comparison with the calculated spot centroid, the error in beam accuracy can be easily calculated. Each calculated centroid has two values, one in the X axis and the other in the Y axis. For the X coordinates, positive deviation value means that the spot shifted to left. For negative value, the spot shifted to right. For the Y coordinates, positive deviation value means that the spot is up shifted. For negative value, the spot is down shifted. Spot centroid shift directions according to deviation values from the target centre are illustrated in Table 1. For real evaluation of reflected solar beam accuracy, an outdoor test is discussed in Section 5.

The automatic calculation of the distance between the centre of the target and the sunbeam centroid could serve as feed-back information for adjustment purposes of calibration and control of heliostat tracking systems. These systems seek to minimise centering error and increase the beam accuracy. The calculated errors in beam accuracy in the X axis and the Y axis are considered as direct calculations of the required displacements of the motors of the heliostats. These calculations are sent to the central control system to perform the correction. This point will be subject of a deeper study, and some field test will be performed in a future work.

3. Optical Quality

The optical quality is evaluated by the calculation of the amount of deviation between light concentrations in the captured solar flux and the concentrations of the designed or calibrated solar flux map. The proposed methodology can be applied to evaluate the whole captured solar flux map or specific regions in it. Different evaluated areas are determined by applying different threshold values. This is useful for flux analysis in actual applications, where different regions of interest in the reflected flux, e.g., borders of the light spot, can be analysed individually. Fig. 5 shows binary images of the image of Fig. 4a created by applying different threshold values. The image of Fig. 5a can be used for the evaluation of the whole light spot because the applied threshold value results in including all pixels that represent the whole spot. The applied threshold value in Fig. 5b allows only representing the centered area which can be evaluated separately. In Fig. 5c, two threshold values are applied to make edges of the solar spot the area of interest in the evaluation process.

In the present work, the solar flux distribution error percentage is a measure of the optical quality evaluation, and it is calculated based on the comparison between the distribution of the captured image and the distribution of a reference image. The reference image is the image of the designed flux distribution. This reference image can be a required calibrated flux distribution map in actual applications. The following section discusses in detail the proposed steps to calculate the error percentage in the flux distribution.

Table 1. Shift direction according to deviation value.

Axis	Deviation Value	Shift Direction
X	Positive	Left
	Negative	Right
Y	Positive	Up
	Negative	Down

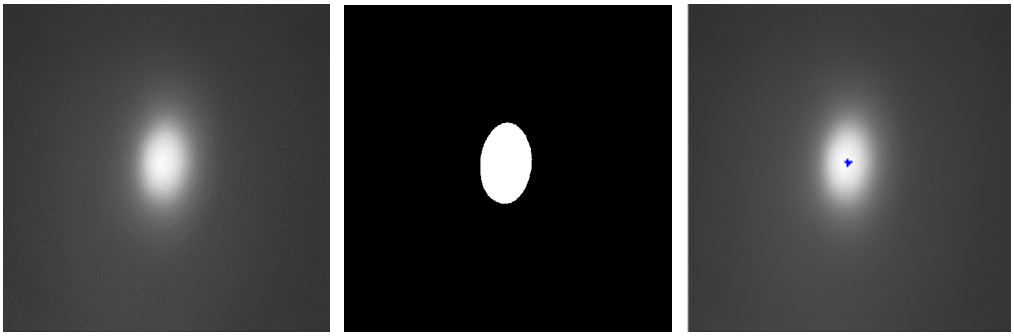

(a) (b) (c)

Fig. 4. (a) HDR image of light spot after perspective correction. (b) Binary image of light spot. (c) Grayscale image of light spot with mark of spot centroid location.

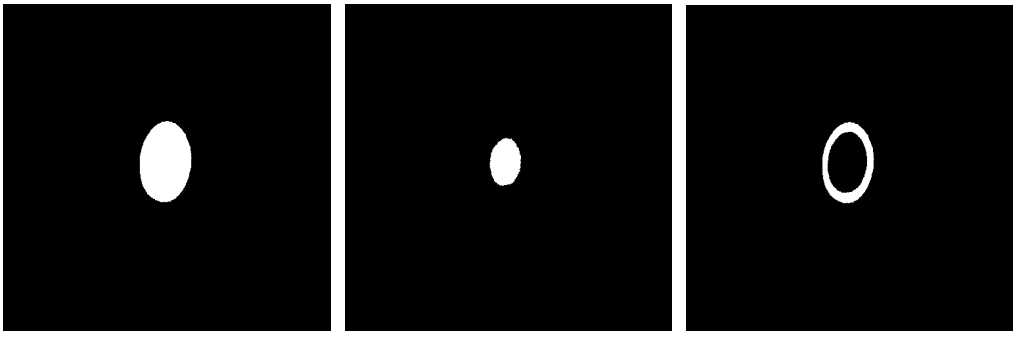

(a) (b) (c)

Fig. 5. Binary images applying: (a) low threshold value, (b) high threshold value and (c) two different threshold values.

3.1. *Distribution Error Percentage Proposed Algorithm*

The deviations in flux distribution between the captured image and the reference image can be evaluated using the following proposed steps:

- Calculate the deviation of each pixel value from the maximum pixel value in the area of interest. This deviation is referred to as DR_i for reference image and DC_j for captured image. They are calculated using Eq. (4) and Eq. (5).

$$DR_i = yr_{max} - yr_i \quad (4)$$
$$DC_j = yc_{max} - yc_j \quad (5)$$

  Where yr_{max} is the maximum pixel value in the reference image and yc_{max} is the maximum pixel value in the captured image.

- Calculate the average of deviations using Eq. (6) and Eq. (7).

$$ADR = \left(\sum_{i=1}^{n} DRi\right)/n \quad (6)$$
$$ADC = \left(\sum_{j=1}^{m} DCj\right)/m \quad (7)$$

  Where *ADR* is the average of deviations in the reference image and *ADC* is the average of deviations in the captured image. The number of pixels in the reference and captured images are *n* and *m*, respectively.

- Calculate the ratio between the average of deviations and the maximum pixel value in the image using Eq. (8) and Eq. (9).

$$ADRM = ADR/yr_{max} \quad (8)$$
$$ADCM = ADC/yC_{max} \quad (9)$$

  Where *ADRM* is the ratio between the average of deviations and the maximum pixel value in the reference image and *ADCM* is the ration between the average of deviations and the maximum pixel value in the captured image.

- Calculate the distribution error percentage (*Error %*) using Eq. (10).

$$Error\ \% = \frac{ADRM - ADCM}{ADRM} * 100\% \quad (10)$$

Positive error values mean that, as compared to the reference image, the captured solar flux is highly concentrated in the evaluated area, while the negative error values indicate that the solar flux is low concentrated at the evaluated area. The grayscale image assigns low pixel values at low concentration areas, thus results in an increase in DC_j, *ADC*, and *ADCM* values. Increasing these values leads to negative error value and the opposite at high concentration areas.

4. Proposed Methodology Validation

The main aim of this section is to validate the proposed methodology for evaluation of beam accuracy and optical quality. The validation process is an important step before the application of the methodology in actual systems. After validation process, the methodology has been used to evaluate real solar flux incident on a calibration target in an outdoor test, which simulates evaluation of real SCR systems, as will be discussed in Section 5.

For validation, the methodology has been applied on grayscale images with known centres and distributions. As illustrated in [22] and [23], the flux distribution of the solar flux reflected onto a flat receiver often approximates a near Gaussian distribution. Therefore, the reference image has been created using MATLAB, where a 2D Gaussian distribution has been converted to a grayscale image with the same size of the evaluated images. Fig. 6 shows the created reference image.

For performing the process, images with different pixel ranges and different illumination levels are evaluated. Fig. 7a shows an image with a uniform Gaussian distribution as the distribution of the reference image but with lower illumination levels. Fig. 7b shows an image with also a uniform Gaussian distribution but with low pixel range. Fig. 7c shows an image with the same distribution of the reference image distribution, but the pixels of the above left quarter are assigned to be zero. The images of Fig. 7a, Fig. 7b and Fig. 7c are known light spot centre and distribution. These images have been created using MATLAB. Fig. 7d shows a merged HDR image from two low dynamic range images, captured by the calibrated double-CCD camera, after perspective correction. The image of Fig. 7d was captured with the same technique of capturing the image of Fig. 4a.

The proposed methodologies in Sections 2 and 3 have been applied to determine spot centroid deviations and distribution error percentage for images of Fig. 7. Calculations have been performed with different threshold values. Applying different threshold values allows evaluating different regions of the light spot. Using Eq. (3), changing the threshold factor changes the threshold value. In the present test, threshold factors of 0.4, 0.6 and 0.8 have been used. Results are presented in Table 2.

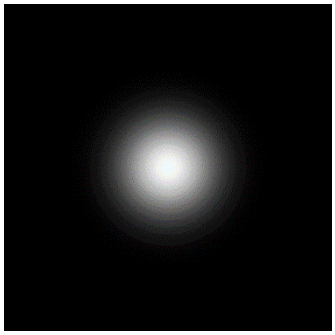

Fig. 6. Reference image simulated by MATLAB.

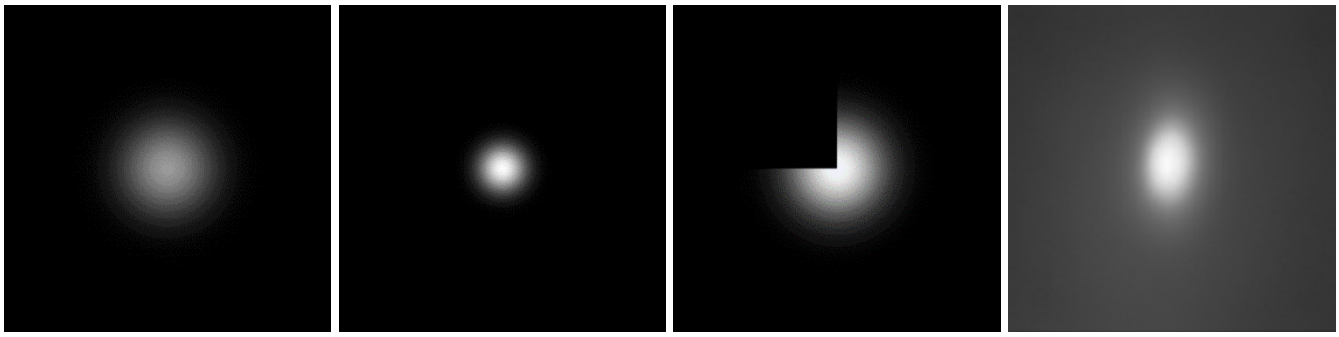

(a) (b) (c) (d)

Fig. 7. (a) Image with low illumination levels. (b) Image with low illumination levels and low pixel range. (c) Image with black quarter. (d) HDR image of a light spot.

Table 2. Spot centroid deviations and distribution error percentage, at different threshold values, for images of Fig. 7.

Image	Threshold Factor	Centroid Error (pixels)		Distribution Error %
		X	Y	
a	0.4	0	0	0
	0.6	0	0	0
	0.8	0	0	0
b	0.4	0	0	0
	0.6	0	0	0
	0.8	0	0	0
c	0.4	-9.59913396	-9.59913396	0
	0.6	-7.169309547	-7.169309547	0
	0.8	-4.753197893	-4.753197893	0
d	0.4	2.6340829	6.502964703	-13.72986494
	0.6	3.238182773	8.375393908	1.544143293
	0.8	4.468245125	8.929247911	-2.805548925

Table 2 shows deviations of centroids of images of Fig. 7 from the centroid of the reference image of Fig. 6 at different threshold values. It also shows distribution error percentage for images of Fig. 7 in comparison with the distribution of the reference image of Fig. 6 at different threshold values. In comparison with the designed reference case, results of Table 2 are as expected:

- For the image of Fig. 7a, although illumination levels of the evaluated area are not the same as illumination levels of the same area in the reference image, distribution is still uniform, leading to zero distribution error percentage. The centroid error also assigns zero value because the centre of the Gaussian distribution of that image is the same as of the reference image.

- For the image of Fig. 7b, although the pixel range of the Gaussian distribution of that image is lower than that of the reference image, the distribution uniformity is still the same. And therefore, both centroid error and distribution error percentage assign zero values.

- For the image of Fig. 7c, although the spot centroid has been shifted, the distribution is still the same as of the reference image. That happens because the black quarter out of the area of interest of the evaluation process due to thresholding.

- For the image of Fig. 7d, the centroid has been shifted and the distribution error percentage assigns non-zero value because the light spot of that image has been created by a lamp that has been directed manually to the centre of the target.

5. Demonstration for Outdoor Test Application

5.1. Experimental Boundary Conditions

For real solar flux evaluation, a mirror with a 546 cm^2 reflecting area was analysed. The mirror was tracked on a 40 x 36 cm flat target facing south. The target was mounted 190 cm above ground level. The mirror was mounted 25 cm above ground level and 400 cm from the plane of target. The mirror simulates a heliostat, and the target simulates the calibration target in real field. The double-CCD camera was used for capturing images. The position of the camera was adjusted in such a way that the captured image can show the target. The camera was connected to a laptop that has the JAI control tool installed. The capturing system was installed at about a 300 cm distance from the target. The test was performed on the rooftop of the National Renewable Energy Centre of Spain (CENER) (Pamplona, Spain) at 42.81799° latitude and -1.644180° longitude. The capturing process was performed at 1 pm on 12 September. Fig. 8 shows the set-up of the test.

For applying the beam accuracy and optical quality proposed calculation methods, the target was captured without reflected light from the mirror, and then two images with different exposure times for the reflected light by the mirror on the target were captured. The two images were merged to a HDR one using the proposed methodology presented in [17]. Fig. 9 shows images of the target after and before reflecting sunlight by the mirror. Fig. 10 shows the images after applying mask to discard parts of the image that are not of our interest.

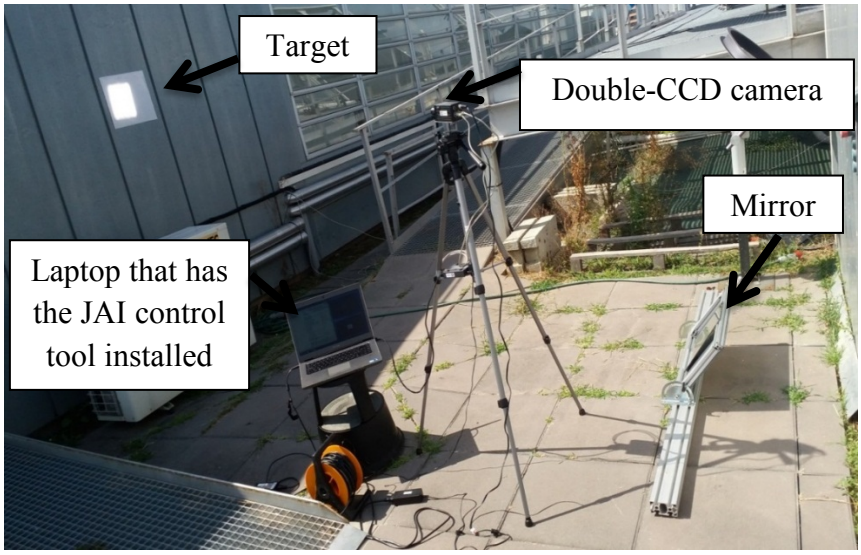

Fig. 8. Set-up of the outdoor test.

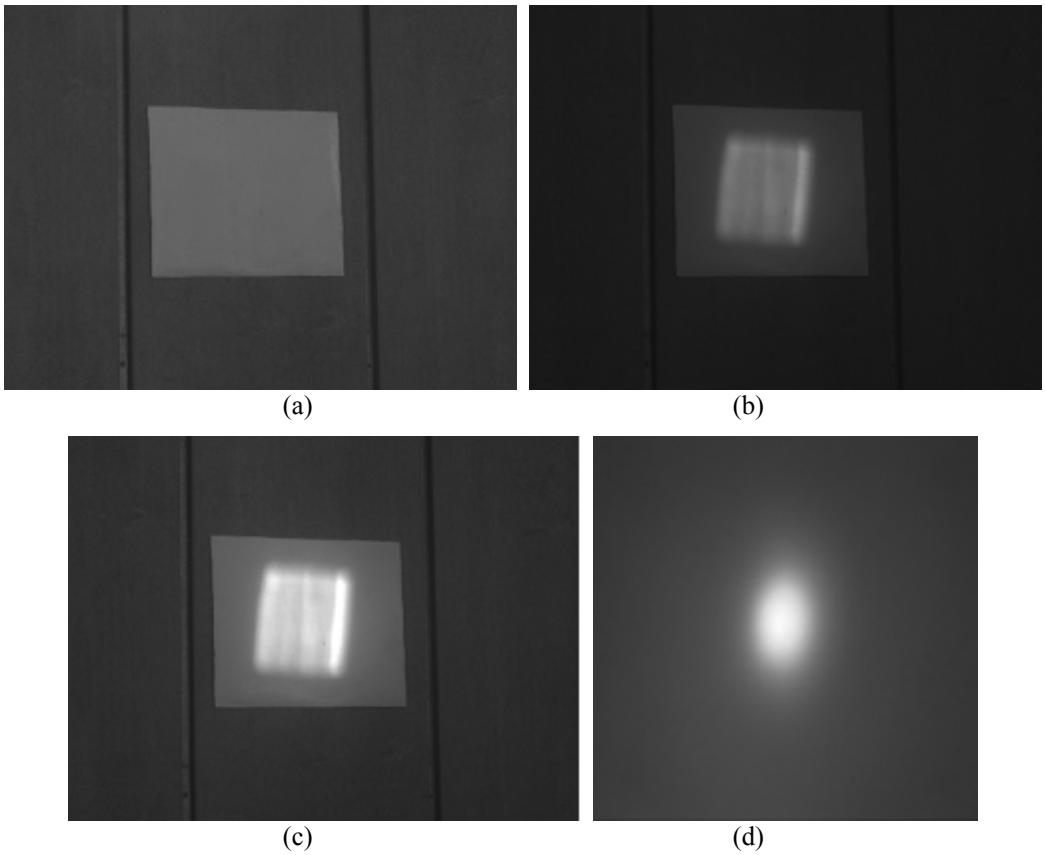

Fig. 9. (a) Target image. (b) Image with 2.5 milliseconds exposure time. (c) Image with 5 milliseconds exposure time. (d) Merged HDR image.

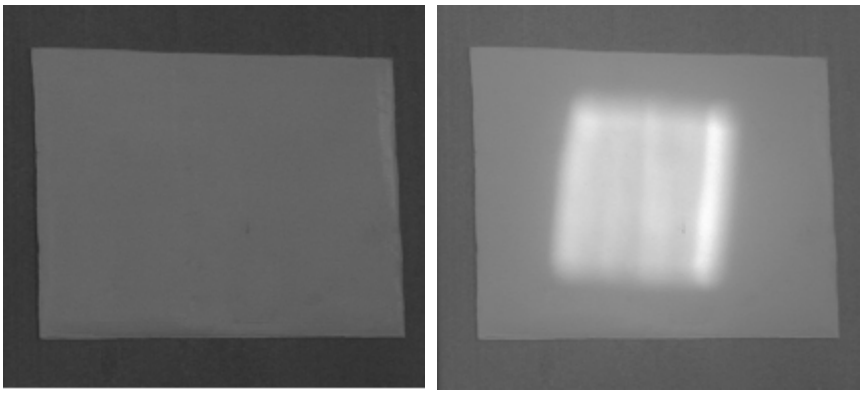

(a) (b)

Fig. 10. Masked images: (a) target image and (b) merged HDR image.

5.2. Optical Model

For applying the proposed methodology, a reference solar flux map is required. Therefore, an optical model has been conducted using Tonatiuh Monte Carlo based solar ray tracing software to extract the reference image of the solar flux. Tonatiuh is an object-oriented program written in C++, which has been experimentally validated [24].

In Monte Carlo ray tracing technique, random directions of large number of rays are traced while they interact with a surface. Each of these rays has the same value of energy depending on the input value of solar irradiance. The direction of each ray is determined by probability density functions. Increasing the number of traced rays increases the accuracy and resolution of Monte Carlo ray tracing method. But large number of rays needs more processing time [25]. The acquired energy from rays depends on absorptivity, reflectivity, and emissivity of the surface.

The Monte Carlo algorithm used in Tonatiuh allows collecting scattering and absorption data of each photon simulated. Depending on number of photons and sun position, Tonatiuh directly assigns to each photon a discrete value of energy that represents the power per photon. In the present model, the sun shape has been modeled as Pillbox shape. The number of solar rays used is 10^7 rays. And the concentrating solar ratio used is 0.028. The direct normal irradiation value depends on the defined location, time and date of the test. Table 3 shows the main defined parameters of the created optical model.

The present study focuses on the reflection of the heliostat on the target. Therefore, the optical model created using Tonatiuh consists of a target and a mirror for reflecting incident solar radiation on the target. Fig. 11 shows the created optical model in Tonatiuh. Locations of the target and the mirror in (x, y, z) coordinate with respect to (0, 0, 0) coordinate of Tonatiuh are shown in Table 4.

Tonatiuh does not provide a post processing tool, so the output file must be exported and analyzed with another program. In the present work, MATLAB is used to convert the extracted binary file to a grayscale image. The grayscale image is then used as a reference image in the evaluation process.

Table 3. Optical model main parameters.

Dimensions	**Target**	40 x 36 cm
	Mirror	26 x 21 cm
Test location	**Latitude**	42.81799°
	Longitude	-1.644180°
Test time and date	**Time**	12 September
	Date	1:00 PM
Sun shape		Pillbox shape
Number of rays		10^7 rays
Concentrating solar ratio		0.028

Table 4. Target and mirror locations in Tonatiuh optical model.

	x	**y**	**z**
Target	0	1.9 (m)	0
Mirror	0.5 (m)	0.25 (m)	-4 (m)

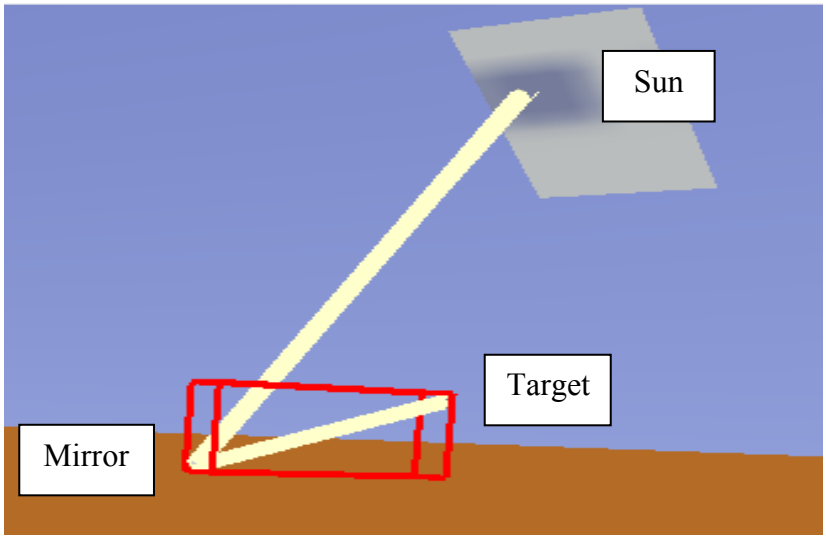

Fig. 11. Tonatiuh optical model.

5.3.Evaluation of Beam Accuracy and Optical Quality

Perspective correction was done for the image of Fig. 10a and applied for the image of Fig. 10b. Fig. 12 shows the reference image and the captured image in grayscale level after preparing for evaluation process. The reference image is the image extracted from Tonatiuh optical model. In order to increase the visibility of details, the grayscale images of Fig. 12 are displayed in 3D false colour images and presented in Fig. 13.

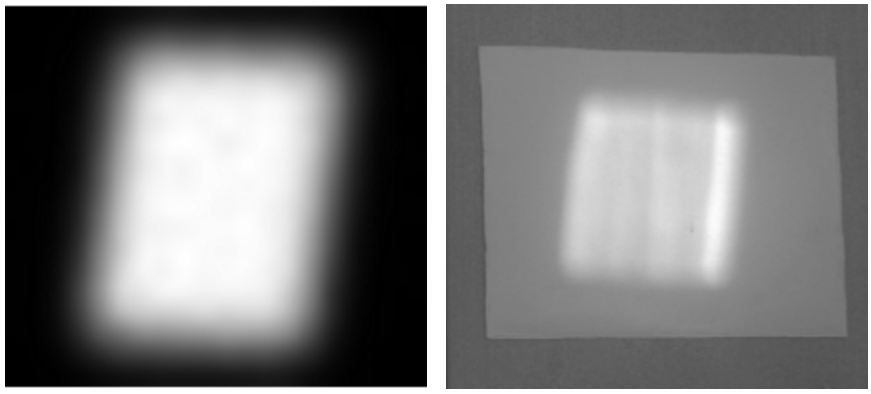

(a) (b)

Fig. 12. Grayscale images: (a) reference image simulated by MATLAB and (b) captured image.

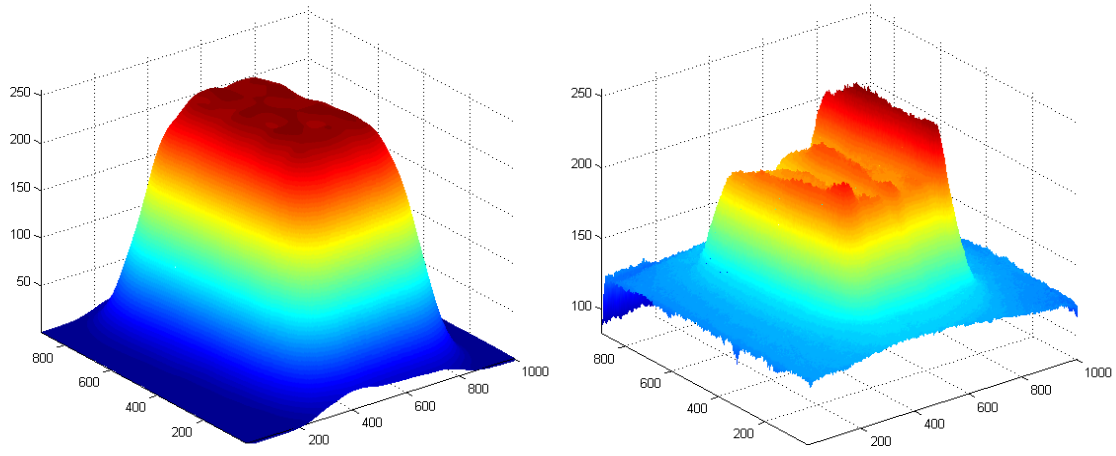

(a) (b)

Fig. 13. 3D false colour images: (a) reference image simulated by MATLAB and (b) captured image.

(a) (b)

Fig. 14. BW Images after applying threshold: (a) reference image and (b) captured image.

For centroid deviation calculation, a threshold was applied using Eq. (3). Fig. 14 shows the two BW images after applying threshold. The centroid of the reflected solar flux on the target was calculated using the proposed methodology of Section 2. It was found that spot centroid deviates from the aiming centre 32 pixels in the horizontal direction and 24 pixels in the vertical direction.

The mirror optical quality has been evaluated using the proposed methodology of Section 3. The system has calculated a –90.90% solar flux distribution error percentage. As discussed before, negative distribution error percentage value means that the concentration of the captured solar flux is lower than that of the reference one. The large variation in flux distribution between the captured image and the reference image can be clearly noted from images of Fig. 13.

In the present system, an interpolation between the number of pixels and the original target dimensions is directly performed to calculate the centroid deviation in length unit. Applying on the present test, it was found that spot centroid deviates from the aiming centre 12.7339 mm in the horizontal direction and 9.6393 mm in the vertical direction. In real SCR plants, in addition to heliostat calibration, the obtained error calculations could serve as feed-back information that allows adjustment purposes of tracking and control systems.

After the application of the technique presented in the present article, its advantages can be summarised as:

- The technique is executed without depending on the capturing system position with respect to the target because it corrects the perspective orientation of the captured images.
- The technique is executed without depending on the target type because it solves problems found on target surface by thresholding and applying filters.
- Calibration target centre is automatically calculated and considered as the aiming point without having to be defined beforehand.
- The technique evaluates the whole captured solar flux map or some parts of it.
- The technique can be applied to evaluate not only the optical performance of one heliostat, but also to evaluate that of whole field.

6. Conclusion

In the present work, an image-based simple and easily applicable methodology to evaluate the beam accuracy and the optical quality of reflected light on a target is presented. The algorithm is executed without depending on the capturing system position and the target type. The algorithm extracts the target from the image and calculates its centre. Then, it calculates the reflected flux map centroid. The beam accuracy is then measured as the deviation of the centroid of the flux map from the target centre. For optical quality measurement, the algorithm measures the distribution of the reflected flux map in comparison with the distribution of reference designed solar flux map. In the present work, the reference solar flux map is conducted using an optical model created by Tonatiuh software. The presented method has been validated by evaluating images of known centroids and distributions.

The present study has contributed in developing simple and effective tools for image analysis relevant to heliostat evaluation and calibration in SCR plants. The developed system accurately analyses the incident solar flux on receivers of SCR systems. In practice, solar flux analysis results are used for control, tracking and calibration of solar systems. It is also used for the evaluation of new system designs and evaluation of expecting solar systems optical performance. The capability of the present methodology for accurate analysis of optical performance of SCR systems has been demonstrated by indoor and outdoor experiments.

Acknowledgements

This work was conducted when one of the authors, Mohamed Adel, was in a study mobility of 12 months at the National Renewable Energy Centre of Spain (CENER). Financial support of MEDSOL project Co-funded by the Erasmus+ programme of the European Union is highly appreciated.

References

[1] A. Pfahl, J. Coventry, M. Röger, F. Wolfertstetter, J. F. Vásquez-Arango, F. Gross, M. Arjomandi, P. Schwarzbözl, M. Geiger, and P. Liedke, "Progress in heliostat development", *Solar Energy*, vol. 152, pp. 3-37, August 2017.

[2] M. Röger, P. Herrmann, S. Ulmer, M. Ebert, C. Prahl, and F. Göhring, "Techniques to Measure Solar Flux Density Distribution on Large-Scale Receivers", *Journal of Solar Energy Engineering*, vol. 136, no. 3, p. 031013, May 2014.

[3] M. R. Rodríguez-Sánchez, C. Leray, A. Toutant, A. Ferriere, and G. Olalde, "Development of a new method to estimate the incident solar flux on central receivers from deteriorated heliostats", *Renewable Energy*, vol. 130, pp. 182-190, January 2019.

[4] E. Thalhammer, "Heliostat Beam Characterization System—Update," *Proceedings of the ISA/79 Conference*, 1979.

[5] A. Imenes, W. Stein, J. Hinkley, R. Benito, and R. Bolling, "Ray tracing and flux mapping as a design and research tool at the National Solar Energy Centre," *ANZSES 2006 Conference (Australia and New Zealand Solar Energy Society)*, 2006.

[6] C. K. Ho and S. S. Khalsa, "A Photographic Flux Mapping Method for Concentrating Solar Collectors and Receivers," *Journal of Solar Energy Engineering*, vol. 134, no. 4, p. 041004, November 2012.

[7] J. E. Pacheco, R. M. Houser, and A. Newmann, "Concepts to Measure Flux and Temperature for External Central Receivers," *International solar energy conference, Solar engineering*, pp. 595–604, 1994.

[8] M. Demirtas, M. Yesilbudak, S. Sagiroglu and I. Colak, "Prediction of solar radiation using meteorological data", *International Conference on Renewable Energy Research and Applications, ICRERA*, Nagasaki, Japan, pp. 1-4, 11-14 November 2012.

[9] M. Jazayeri, S. Uysal, and K. Jazayeri, "A case study on solar data collection and effects of the Sun's position in the sky on solar panel output characterization in Northern Cyprus", *International Conference on Renewable Energy Research and Applications, ICRERA*, Madrid, Spain, pp. 184-189, 20-23 October 2013.

[10] R. Al-Hajj, A. Assi, and F. Batch, "An evolutionary computing approach for estimating global solar radiation", *International Conference on Renewable Energy Research and Applications, ICRERA*, Birmingham, UK, pp. 285-290, 20-23 November 2016.

[11] W. Yaici, and E. Entchev, "Prediction of the performance of a solar thermal energy system using adaptive neuro-fuzzy inference system", *International Conference on Renewable Energy Research and Applications, ICRERA*, Milwaukee, USA, pp. 601-604, 19-22 October 2014.

[12] E. M. Toygar, A. Yazar, T. Byram, M. Tustan, O. F. Kaya, O. Das, and H. Calmaz, "Design and development of solar flat mirror and heat storage System", *International Conference on Renewable Energy Research and Applications, ICRERA*, Milwaukee, USA, pp. 821-827, 19-22 October 2014.

[13] F. Sun, M. Guo, Z. Wang, W. Liang, Z. Xu, Y. Yang, and Q. Yu, "Study on the heliostat tracking correction strategies based on an error-correction model," *Solar Energy*, vol. 111, pp. 252–263, January 2015.

[14] S. Ulmer, T. März, C. Prahl, W. Reinalter, and B. Belhomme, "Automated high resolution measurement of heliostat slope errors," *Solar Energy*, vol. 85, no. 4, pp. 681–687, April 2011.

[15] "JAI AD-081 GE CCD camera user manual", 2013. [Online]. Available: https://www.jai.com/downloads/manual-ad-081ge. [Accessed: 25 February 2021].

[16] "JAI Camera Software", 2013. [Online]. Available: https://www.jai.com/support-software/jai-software. [Accessed: 25 February 2021].

[17] M. Adel, A. Peña-Lapuente, M. Rady, A. Hamdy, '' Development of a New High Dynamic Range Technique for Solar Flux Analysis Using Double-CCD Optical Camera'', *International Journal of Renewable Energy Research*, vol. 9, no. 2, pp.783-794, June 2019.

[18] M. Berenguel, F. R. Rubio, A. Valverde, P. J. Lara, M. R. Arahal, E. F. Camacho, and M. López, "An artificial vision-based control system for automatic heliostat positioning offset correction in a central receiver solar power plant", *Solar Energy*, vol. 76, no. 5, pp. 563-575, January 2004.

[19] E. Pietka, *Handbook of Medical Imaging: processing and analysis*, 2000.

[20] Y. Guo, A. Sengurb, and J. Ye, "A novel image thresholding algorithm based on neutrosophic similarity score", *Measurement*, vol. 58, pp. 175-186, December 2014.

[21] S. Barnard, "Interpreting perspective images", *Artificial Intelligence*, vol. 21, no. 4, pp. 435-462, November 1983.

[22] F. K. Boese, A. Merkel, D. Stahl, and H. Stehle, "A consideration of possible receiver designs for solar tower plants," *Solar Energy*, vol. 26, no. 1, pp. 1–7, January 1981.

[23] A. Grobler, "Aiming strategies for small central receiver systems," *Stellenbosch University*, 2015.

[24] M. J. Blanco, A. Mutuberria, and D. Martinez, "Experimental validation of Tonatiuh using the Plataforma Solar de Almería secondary concentrator test campaign data," *16th annual SolarPACES symposium*, 2010.

[25] S. Bode, P. Gauche D. Griffith, "A Novel Approach to Reduce Ray Tracing Simulation Times by Predicting Number or Rays", *Energy Procedia*, vol. 49, pp. 2454-2461, 2014.